

JGR Space Physics

RESEARCH ARTICLE

10.1029/2020JA028631

Key Points:

- Quasi-parallel whistler waves excited by anisotropic electrons can evolve into a spectrum with a power gap around $0.5\Omega_e$
- The electrons form a beam-like/plateau distribution in the parallel direction due to the Landau resonance
- The electron beam-like/plateau distribution leads to the severe damping of whistler waves around $0.5\Omega_e$ via cyclotron resonance

Correspondence to:

Q. Lu and X. Gao,
qmlu@ustc.edu.cn;
gaoxl@mail.ustc.edu.cn

Citation:

Chen, H., Gao, X., Lu, Q., Sauer, K., Chen, R., Yao, J., & Wang, S. (2021). Gap formation around $0.5\Omega_e$ of whistler-mode waves excited by electron temperature anisotropy. *Journal of Geophysical Research: Space Physics*, 126, e2020JA028631. <https://doi.org/10.1029/2020JA028631>

Received 28 AUG 2020
Accepted 22 DEC 2020

Gap Formation Around $0.5\Omega_e$ of Whistler-Mode Waves Excited by Electron Temperature Anisotropy

Huayue Chen^{1,2} , Xinliang Gao^{1,2} , Quanming Lu^{1,2} , Konrad Sauer³ , Rui Chen^{1,2} , Jiansheng Yao^{1,2} , and Shui Wang^{1,2} 

¹CAS Key Laboratory of Geospace Sciences, School of Earth and Space Sciences, University of Science and Technology of China, Hefei, China, ²CAS Center for Excellence in Comparative Planetology, Hefei, China, ³Max-Planck-Institute for Solar System Research (up to 2005), Göttingen, Germany

Abstract With a one-dimensional particle-in-cell simulation model, we have investigated the gap formation around $0.5\Omega_e$ of the quasi-parallel whistler-mode waves excited by an electron temperature anisotropy. When the frequencies of excited waves in the linear stage cross $0.5\Omega_e$, or when they are slightly larger than $0.5\Omega_e$ but then drift to lower values, the Landau resonance can make the electron distribution form a beam-like/plateau population. Such an electron distribution only slightly changes the dispersion relation of whistler-mode waves, but can cause severe damping around $0.5\Omega_e$ via cyclotron resonance. At last, the wave spectrum is separated into two bands with a power gap around $0.5\Omega_e$. The condition under different electron temperature anisotropy and plasma beta is also surveyed for such kind of power gap. Besides, when only the waves with frequencies lower than $0.5\Omega_e$ are excited in the linear stage, a power gap can also be formed due to the wave-wave interactions, i.e., lower band cascade. Our study provides a clue to reveal the well-known $0.5\Omega_e$ power gap of whistler-mode waves ubiquitously observed in the inner magnetosphere.

Plain Language Summary The whistler-mode waves, which have a great influence on electron dynamics in the Earth's magnetosphere, are ubiquitously observed with a power minimum around $0.5\Omega_e$. This phenomenon is also called the $0.5\Omega_e$ power gap. How the power gap forms is still one of the remaining issues since whistler waves were in-situ detected by satellites about 50 years ago. In this study, with a PIC simulation model, we propose a promising and natural generation mechanism of the power gap in the quasi-parallel whistler waves. When the frequencies of excited waves in the linear stage cross $0.5\Omega_e$, or when they are slightly larger than $0.5\Omega_e$ but then drift to lower values, a pronounced beam-like/plateau electron distribution in the parallel direction is formed due to the Landau resonance. Such an electron distribution can cause a severe damping around $0.5\Omega_e$ via cyclotron resonance. At last, the power gap naturally generates. Besides, when only the waves with frequencies lower than $0.5\Omega_e$ are excited in the linear stage, a power gap can also be formed due to the wave-wave interactions. Our study can shed light on the formation of $0.5\Omega_e$ power gap in the whistler-mode waves observed in the inner magnetosphere.

1. Introduction

Whistler-mode waves are intense and coherent electromagnetic emissions that naturally occur in the Earth's inner magnetosphere (Burtis & Helliwell, 1969; Chen et al., 2013; Santolík et al., 2005; Tsurutani & Smith, 1974). These waves are believed to play an important role in both scattering low-energy (0.1–30 keV) electrons into the upper atmosphere to produce diffuse aurora (Ni et al., 2008; Thorne et al., 2010) and accelerating energetic (\sim 100 keV) electrons to relativistic energies (>1 MeV) in the heart of Van Allen radiation belt (Thorne et al., 2013; Xiao et al., 2014). One of the most remarkable properties of whistler-mode waves is the power gap around $0.5\Omega_e$ (where Ω_e represents the equatorial electron gyrofrequency; Burtis & Helliwell, 1969; Gao et al., 2019; Li et al., 2011; Santolík et al., 2003; Tsurutani & Smith, 1974), which can separate their spectrograms into an upper band (0.5–0.8 Ω_e) and a lower band (0.1–0.5 Ω_e).

Although great efforts have been devoted to explain the formation of the power gap in the past several decades (Gao et al., 2016; Li et al., 2019; Liu et al., 2011; Omura et al., 2009; Ratcliffe & Watt, 2017), there is still no consensus on this issue. It is naturally thought that the upper band and lower band of the whistler-mode waves are excited by two different anisotropic electron populations (Fu et al., 2014; Li et al., 2019; Liu

et al., 2011). However, the two different electron populations should be chosen carefully to make the power gap around $0.5\Omega_e$. The idea of nonlinear wave-wave interactions has also been introduced to explain such banded whistler-mode waves, where the harmonics of whistler-mode waves are produced due to the lower band cascade, and the “multiband chorus” commonly observed in the magnetosphere is then formed (Chen et al., 2017; Gao et al., 2016, 2017). Whistler-mode waves are expected to experience enhanced nonlinear damping via the Landau resonance around $0.5\Omega_e$ as they propagate toward higher latitudes from the source region (Hsieh & Omura, 2018; Omura et al., 2009), suggesting that banded spectra of whistler-mode waves tend to appear off the equator. However, a recent statistical study (Gao et al., 2019) showed that banded spectra of whistler-mode waves are preferentially observed near the magnetic equator.

In this study, by performing a self-consistent kinetic simulation model, we try to figure out the physical process underlying the formation of banded whistler-mode waves with a clear power gap. After the excitation of whistler-mode waves, there is a pronounced beam-like/plateau electron component generated, which is suggested to play a key role in the gap formation around $0.5\Omega_e$.

2. Simulation Model and Initial Setup

A one-dimensional (1-D) particle-in-cell (PIC) simulation model with periodic boundary condition is employed in this study to investigate the evolution of whistler-mode waves excited by an electron temperature anisotropy. This model allows spatial variations only in the x direction, meaning that the wave vector will be fixed along the x axis, but includes three components of electromagnetic fields and velocities. The full dynamics of particles are obtained by solving the relativistic motion equation. The electric and magnetic fields are defined on grids and calculated by integrating the time-dependent Maxwell equations with a fully explicit “Leapfrog” algorithm (Birdsall & Langdon, 1991). Although according to the linear theory the whistler-mode waves along the background magnetic field have the maximum growth rate, satellite observations have shown that these waves are in general not parallel propagating in the Earth’s magnetosphere, even in the equatorial region. Statistical results have demonstrated that the wave normal angle of the whistler-mode waves ranges between 0° and 30° in their source region (Gao et al., 2018; Li et al., 2011). Therefore, in our simulation model, the wave normal angle of excited waves is fixed as $\theta = 20^\circ$, and the background magnetic field $\vec{B}_0 = B_0(\cos\theta\hat{x} + \sin\theta\hat{z})$ is lying in the x - z plane.

The simulation box is assumed to be located in the source region of whistler-mode waves. In our simulations, the ions are motionless, and there are two kinds of electrons: the cold electrons and tenuous warm electrons, which are denoted by the subscripts “c” and “w,” respectively. The cold electrons satisfy the isotropic Maxwell distribution with the plasma beta of $\beta_c = 2\mu_0 n_0 k_B T_c / B_0^2 = 10^{-4}$. The velocity distribution of warm electrons is assumed to be bi-Maxwellian, and they provide the free energy for wave excitation (Chen et al., 2017, 2018; Fu et al., 2014; Lu et al., 2004, 2019). The densities of the cold and warm electrons are $0.85n_0$ and $0.15n_0$ (Gao et al., 2014; where n_0 denotes the total plasma density), respectively. In the Earth’s magnetosphere, the typical values of the background magnetic field and total plasma density at L -shell = 7 are $B_0 = 90$ nT and $n_0 = 1.26$ cm $^{-3}$, respectively. Then, the ratio between electron plasma frequency and gyrofrequency is given as $\omega_{pe} / \Omega_e = 4.0$. The grid size is $\Delta x = 0.18c / \omega_{pe}$ ($\approx 2.4\lambda_{De}$, where c / ω_{pe} is the electron inertial length and λ_{De} is the Debye length of the warm electrons), and the grid number is 3072, i.e., the length of the simulation box is $553c / \omega_{pe}$. The time step is $\Delta t = 0.025\Omega_e^{-1}$. In order to reduce the noise level, we uniformly set average 7,000 macroparticles in every cell for each species.

3. Simulation Results

In this paper, we will first run the case, where the temperature anisotropy and plasma beta of the tenuous warm electrons are $T_{\perp w} / T_{\parallel w} = 4.0$ and $\beta_{\parallel w} = 2\mu_0 n_0 k_B T_{\parallel w} / B_0^2 = 0.09$, to demonstrate the gap formation around $0.5\Omega_e$ due to the process related to the Landau resonance. If there is no explicit statement, the simulation results are obtained with these parameters. The evolution of whistler-mode waves is overviewed in Figure 1a, which displays the k - t spectrogram of transverse fluctuating magnetic fields $\delta B_t^2 / B_0^2$

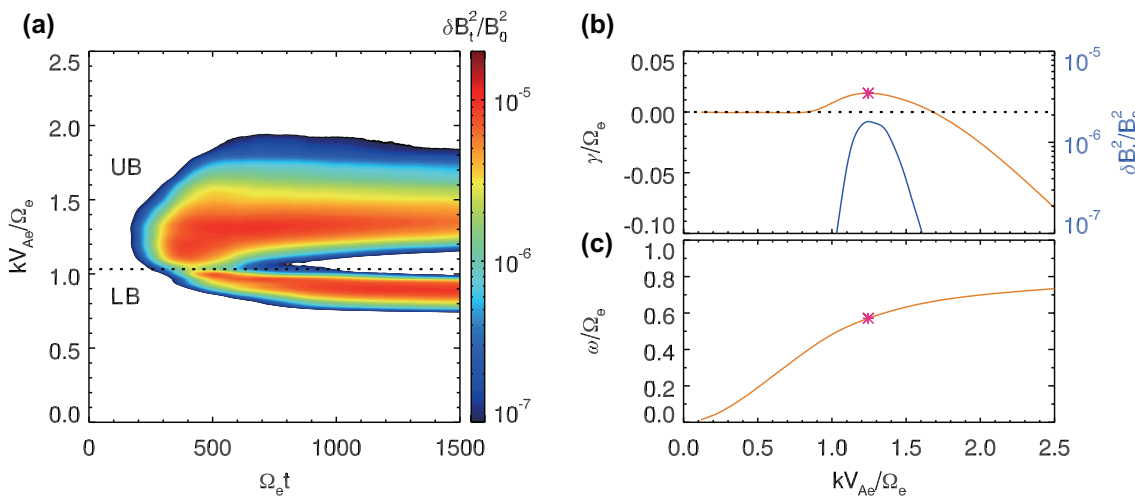


Figure 1. (a) The k - t spectrogram of transverse fluctuating magnetic fields $\delta B_t^2 / B_0^2$, with the black dotted line marking the wave number ($kV_{Ae} / \Omega_e = 1.03$) corresponding to $0.5\Omega_e$; the (b) growth rate and (c) dispersion relation of whistler-mode waves calculated by the linear theory with initial setup, where the wave modes with the maximum growth rate are denoted by magenta stars. In Figure 1b, the blue line represents $\delta B_t^2 / B_0^2$ as a function of kV_{Ae} / Ω_e at $\Omega_e t = 250$.

($\delta B_t^2 = \delta B_y^2 + \delta B_z^2$). The dotted line marks the wave number ($kV_{Ae} / \Omega_e = 1.03$) corresponding to the frequency $0.5\Omega_e$ for reference. At first, the whistler-mode waves with the dominant frequency $\omega / \Omega_e = 0.58$, corresponding to the wave number of $kV_{Ae} / \Omega_e = 1.24$, are excited by the anisotropic warm electrons at about $\Omega_e t = 150$, and their amplitude increase till $\Omega_e t \approx 550$. Simultaneously, the wave frequencies drift to smaller values, which is attributed to the following quasilinear process: with the reduced anisotropy of the warm electrons due to the scattering by the excited waves, the wave frequencies also decrease (Sydora et al., 2007). The power gap around $0.5\Omega_e$ starts to appear at $\Omega_e t \approx 450$, and becomes obvious after $\Omega_e t \approx 800$. Then, the wave spectrum has two separate bands: the upper band whose frequencies are larger than $0.5\Omega_e$, and the lower band whose frequencies are smaller than $0.5\Omega_e$. The power gap between the lower and upper bands is continuously widening till the end of the simulation. Figures 1b and 1c provide the growth rate and dispersion relation of whistler-modes calculated by the linear theory model with the initial plasma parameters (Xie & Yong, 2016). The $\delta B_t^2 / B_0^2$ as a function of kV_{Ae} / Ω_e at $\Omega_e t = 250$ is also given in Figure 1b, which can be well described by the linear growth rate. The peak power of $\delta B_t^2 / B_0^2$ is consistent with the dominant wave mode (the wave mode with the maximum growth rate), i.e., $kV_{Ae} / \Omega_e = 1.24$ and $\omega / \Omega_e = 0.58$ (magenta stars).

The whistler waves with a power gap at $0.5\Omega_e$ are generated in our model, which are quite similar to those detected in the Earth's magnetosphere. To understand how the gap forms, we further analyze the evolution of warm electron distribution. Present operating satellites (such as THEMIS, Van Allen Probes) in the magnetosphere cannot provide the electron distribution function with sufficiently high time resolution and accuracy, but simulations can. Figure 2 illustrates the temporal evolution of warm electron velocity distributions in the (a) parallel and (b) perpendicular directions. The whistler waves are excited by the electron temperature anisotropy, and the perpendicular temperature decreases with time as shown in Figure 2b. However, it still remains as a Gaussian shape. While, in the parallel direction, the electron velocity distribution is found to change much. Besides the parallel heating, there is a pronounced beam-like/plateau component forming at about $\pm 0.5V_{Ae}$ after the excitation of the whistler waves. This beam-like/plateau component is resulted from the Landau resonance between the warm electrons and whistler waves in the two bands, since linear theory tells that the Landau resonance velocities of whistler waves are all close to $\pm 0.5V_{Ae}$. This scenario is supported by a recent statistical study using THEMIS data, which also shows the beam-like/plateau electron components are usually observed along with whistler waves (Chen et al., 2019).

Then, we have further investigated the effects of beam-like/plateau electron component on the existing whistler-mode spectrum via a linear theory model. The power gap at $0.5\Omega_e$ first appears at $\Omega_e t \approx 450$

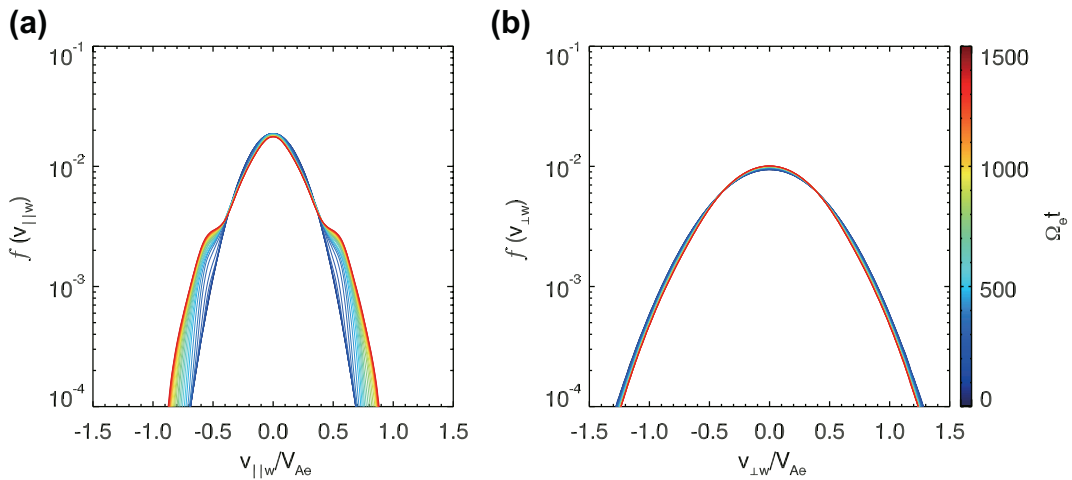


Figure 2. The temporal evolution of warm electron velocity distributions in the (a) parallel and (b) perpendicular directions, in which the coded colors represent different times.

(Figure 1a) when the beam-like/plateau electron component becomes discernible (Figure 2a). Figures 3a and 3b exhibit the velocity distributions of warm electrons at $\Omega_e t = 450$ in parallel and perpendicular directions, respectively. The velocity distribution of warm electrons at $\Omega_e t = 450$ can be fitted by a summation of bi-Maxwellian distributions as $f = \sum_i f_i$, where

$$f_i = \frac{n_i}{\pi^{3/2} v_{||th,i} v_{\perp th,i}^2} \exp\left(-\frac{(v_{||} - v_{b,i})^2}{v_{||th,i}^2} - \frac{v_{\perp}^2}{v_{\perp th,i}^2}\right) \quad (1)$$

Here, $v_{||}$ and v_{\perp} are the parallel and perpendicular velocities, and $v_{||th,i}$ and $v_{\perp th,i}$ are the parallel and perpendicular thermal velocities of i component. The beam velocity and number density of each component are represented by $v_{b,i}$ and n_i , respectively. With the least square method, we choose four components (i.e., $i = 4$) to fit the velocity distribution of warm electrons. The fitting parameters are listed in Table 1 and the fitted curves are plotted as the blue lines in Figures 3a and 3b. Note that the velocity distribution of cold electrons remains almost unchanged. The corresponding growth rate and dispersion relation are given in Figures 3c and 3d, and the results for initial setup are over plotted for comparison. The effects of beam-like/plateau component can be found in two aspects. On the one hand, the dispersion relation of whistler waves has been a little bit distorted around $0.5\Omega_e$ (Figure 3d). On the other hand, the growth rate around $0.5\Omega_e$ now becomes negative, but those of both the lower band and upper band waves still remain positive. It means that whistler-mode waves are heavily damped around $0.5\Omega_e$ when the velocity distribution of the warm electrons has a beam-like/plateau component in the parallel direction, which has recently been described in Sauer et al. (2020). Moreover, since the density of the beam-like/plateau electron component increases with time (Figure 2b), the frequency range of waves with a negative growth rate gets wider and wider (not shown). This can well explain the gradual widening of the power gap with time till the end of the simulation.

The energy transfer between whistler waves and warm electrons during the entire evolution can be described by $P = \sum_{i=1}^{nx} \delta \vec{E} \cdot \vec{j} / N$, where $\delta \vec{E}$, \vec{j} , and N denote the wave electric field, current density, and the number of warm electrons, and Σ means a summation of all the grid cells. Figure 4 illustrates the (a) total wave power, (b) $P_{||} = \sum_{i=1}^{nx} \delta E_{||} j_{||} / N$, and (c) $P_{\perp} = \sum_{i=1}^{nx} \delta E_{\perp} j_{\perp} / N$ for three ranges of wave modes: the upper band with $|kV_{Ae}| / \Omega_e = 1.20 - 1.30$ (blue), around the gap with $|kV_{Ae}| / \Omega_e = 1.00 - 1.10$ (green), and the lower band with $|kV_{Ae}| / \Omega_e = 0.85 - 0.95$ (red). Note that the positive (or negative) P means that the energy is transferred from waves (warm electrons) to warm electrons (waves). Via the cyclotron resonance with warm electrons, the upper-band waves are first excited (Figure 4a), whose free energy is gained only from

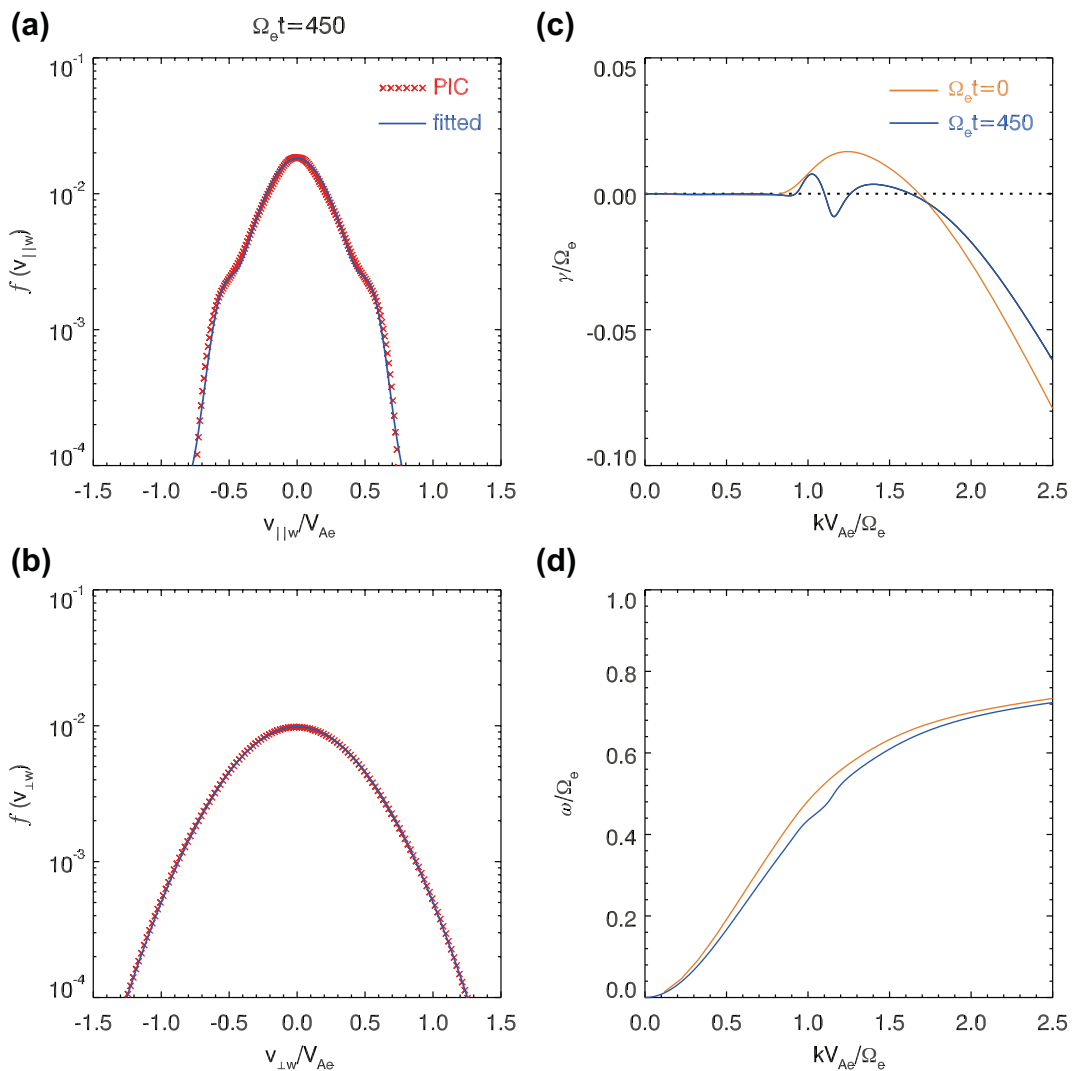


Figure 3. The fitted electron velocity distribution at $\Omega_e t = 450$ (blue lines) in the (a) parallel and (b) perpendicular directions. The velocity distributions in the simulation model are over plotted by red crosses. The (c) linear growth rate and (d) dispersion relation at $\Omega_e t = 0$ and $\Omega_e t = 450$ are displayed by orange and blue lines, respectively.

the perpendicular direction (Figure 4c). The waves around the gap and in the lower band are sequentially generated in the same way (Figures 4a and 4c). While, in the parallel direction, the energy is always transferred from the whistler waves to the warm electrons as long as the waves exist (Figure 4b), suggesting that the beam-like/plateau electron component should be contributed by all three ranges of wave modes via the

Landau resonance. Most notably, the sign of P_\perp associated with the waves around the gap suddenly turns into a positive value at $\Omega_e t \approx 450$ (Figure 4c), just when the power gap appears in the spectrum (Figure 1a) and the beam-like/plateau component electron distribution becomes obvious (Figure 2a). This reveals that the strong damping of the waves around $0.5\Omega_e$ caused by the beam-like/plateau electron component mainly occurs in the perpendicular direction. Here, we don't know whether this strong wave damping is caused by the cyclotron resonance or by the Landau resonance. For the waves propagating in the parallel ($+x$) direction, the cyclotron resonant velocity is $V_c = -0.516V_{Ae}$ and the Landau resonant velocity is $V_L = 0.516V_{Ae}$. While for the waves propagating in the

Table 1

The Fitting Parameters of the Velocity Distribution of Warm Electrons at $\Omega_e t = 450$ Shown in Figures 3a and 3b

	n_t / n_0	$v_{ th} / V_{Ae}$	$v_{\perp th} / V_{Ae}$	v_b / V_{Ae}
#1	11.0985%	0.2859	0.5480	0.0
#2	3.8148%	0.4523	0.5129	0.0
#3	0.04335%	0.1023	1.0629	0.532
#4	0.04335%	0.1023	1.0629	-0.532

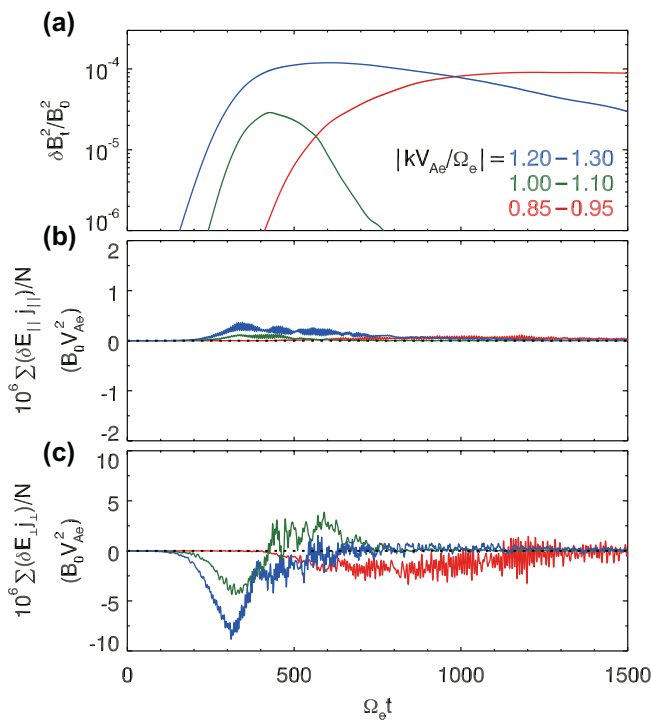


Figure 4. The temporal evolution of (a) total wave power, (b) $P_{\parallel} = \sum_{i=1}^{nx} \delta E_{\parallel i} / N$, and (c) $P_{\perp} = \sum_{i=1}^{nx} \delta E_{\perp i} / N$ for three ranges of wave modes: upper band with $|kV_{Ae} / \Omega_e| = 1.20 \sim 1.30$ (blue), around the gap with $|kV_{Ae} / \Omega_e| = 1.00 \sim 1.10$ (green), and lower band with $|kV_{Ae} / \Omega_e| = 0.85 \sim 0.95$ (red).

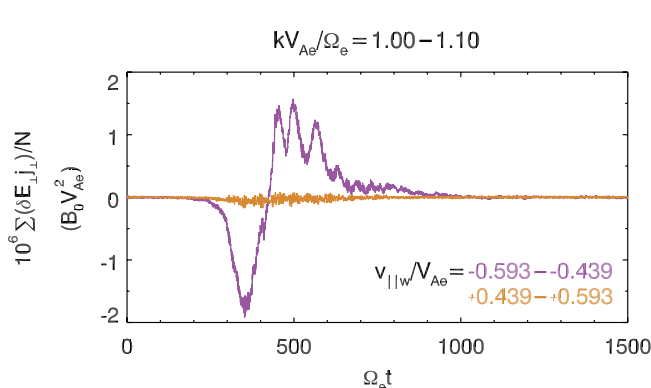


Figure 5. The temporal evolution of energy transfer between warm electrons and the waves around the gap (with $kV_{Ae} / \Omega_e = 1.00 \sim 1.10$) in the perpendicular direction via cyclotron resonance ($P_{\perp c}$) and Landau resonance ($P_{\perp L}$), which are represented by the magenta and orange lines, respectively.

antiparallel (-x) direction, $V_c = 0.516V_{Ae}$ and $V_L = -0.516V_{Ae}$. Therefore, for the waves propagating in both directions, the damping via the cyclotron resonance and via Landau resonance cannot be distinguished.

The waves propagating in the parallel direction and in the antiparallel direction have then been separated, following the method in Terasawa et al. (1986). We have further calculated the energy transfer between the resonant electrons and the waves propagating in the parallel direction with $kV_{Ae} / \Omega_e = 1.00 - 1.10$, by using the same algorithm described above. The current densities (j) associated with the cyclotron resonant electrons and the Landau resonant electrons are then estimated in the ranges of $-0.593V_{Ae}$ to $-0.439V_{Ae}$, and $0.439V_{Ae}$ to $0.593V_{Ae}$, respectively. Figure 5 illustrates the energy transfer in the perpendicular direction via cyclotron resonance ($P_{\perp c}$, denoted by the magenta line) and Landau resonance ($P_{\perp L}$, represented by the orange line). It is shown the $P_{\perp c}$ is negative in the wave growth phase ($\Omega_e t \approx 200 - 450$), indicating the waves are excited via cyclotron resonance. After $\Omega_e t \approx 450$, $P_{\perp c}$ turns into a significant positive value, which can contribute to the severe wave damping. However, the energy transfer in the perpendicular direction via Landau resonance is quite weak ($P_{\perp L} \approx 0$). Therefore, the wave damping around $0.5\Omega_e$ is mainly due to the cyclotron resonance.

We have also investigated how the plasma beta ($\beta_{\parallel w}$) and temperature anisotropy ($T_{\perp w} / T_{\parallel w}$) of warm electrons affect the gap formation. Figure 6 exhibits the k - t spectrogram of $\delta B_t^2 / B_0^2$ for the cases with (a) $\beta_{\parallel w} = 0.04$, (b) $\beta_{\parallel w} = 0.09$, and (c) $\beta_{\parallel w} = 0.12$, where the temperature anisotropy is fixed at $T_{\perp w} / T_{\parallel w} = 3.5$. The dominant frequencies in these cases are $\omega / \Omega_e = 0.642, 0.566$, and 0.540 , respectively. It is worth noting that the dominant frequency of excited waves is much higher than $0.5\Omega_e$ in the case with $\beta_{\parallel w} = 0.04$. For the cases with $\beta_{\parallel w} = 0.09$ and $\beta_{\parallel w} = 0.12$ shown in Figures 6b and 6c, there are significant banded whistler-mode spectra with a power gap near $0.5\Omega_e$. While, in the case with $\beta_{\parallel w} = 0.04$ (Figure 6a), the generated whistler waves only appear in the frequency band higher than $0.5\Omega_e$, and will not drift to the frequency band lower than $0.5\Omega_e$. Figure 7 displays the k - t spectrogram for the cases with (a) $T_{\perp w} / T_{\parallel w} = 2.5$, (b) $T_{\perp w} / T_{\parallel w} = 3.5$, and (c) $T_{\perp w} / T_{\parallel w} = 5.0$, respectively, where the plasma beta keeps at $\beta_{\parallel w} = 0.15$. The dominant frequencies in these cases are $\omega / \Omega_e = 0.502, 0.521$, and 0.537 , respectively. For the cases with $T_{\perp w} / T_{\parallel w} = 3.5$ and $T_{\perp w} / T_{\parallel w} = 5.0$ (Figures 7b and 7c), both lower-band and upper-band waves can be generated, and the banded spectra can last till the end of the simulation. While, in the case with $T_{\perp w} / T_{\parallel w} = 2.5$ (Figure 7a), although the banded whistler spectrum can be formed at $\Omega_e t \approx 1000$, the upper band only survives for a very short time due to its small amplitude, resulting in a single frequency band lower than $0.5\Omega_e$. In some cases (Figures 6c, 7b, and 7c), even though the most unstable modes are in the upper band, the lower-band waves also have a considerable growth rate. As a result, the whistler waves are excited in one continuous band at the beginning of simulation. However, the power gap around $0.5\Omega_e$ still forms due to the existence of a beam-like/plateau electron component.

We have further run another case, where the temperature anisotropy and plasma beta of the tenuous warm electrons are $T_{\perp w} / T_{\parallel w} = 4.0$ and $\beta_{\parallel w} = 0.60$. Figure 8a shows the corresponding k - t spectrogram, which also exhibits two separate bands with a gap around $0.5\Omega_e$. Here, the lower band is first excited by anisotropic electrons, and its power peak at $\Omega_e t = 120$ is consistent with the most unstable wave mode

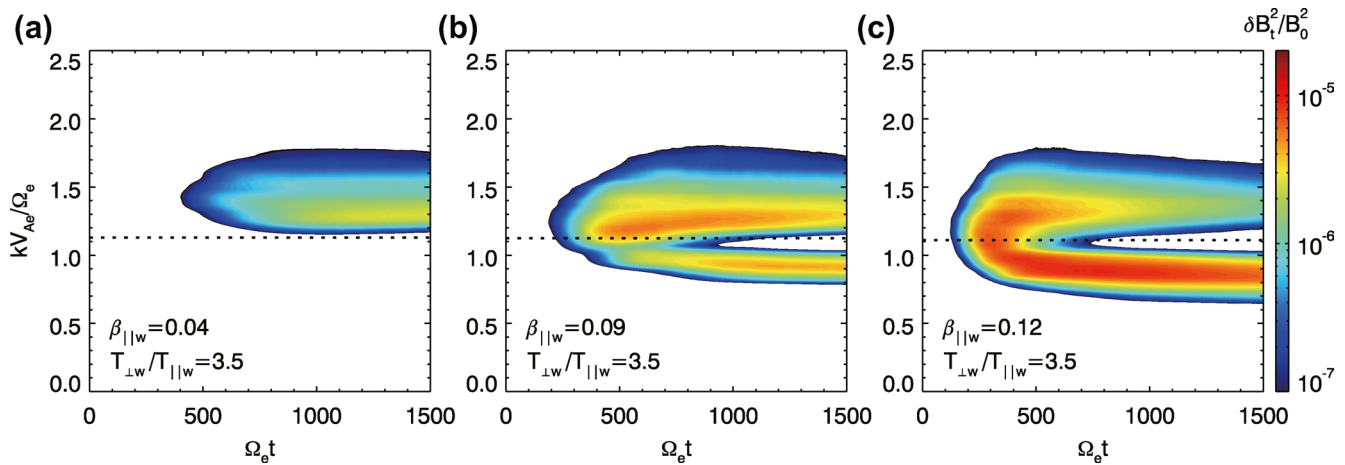


Figure 6. The k - t spectrogram of $\delta B_t^2 / B_0^2$ for the cases with (a) $\beta_{||w} = 0.04$, (b) $\beta_{||w} = 0.09$, and (c) $\beta_{||w} = 0.12$, where the temperature anisotropy is fixed at $T_{\perp w} / T_{||w} = 3.5$. The dotted lines in three panels represent the wave numbers ($kV_{Ae} / \Omega_e = 1.130, 1.125$, and 1.113) corresponding to $0.5\Omega_e$ in each case.

($kV_{Ae} / \Omega_e = 0.84$ and $\omega / \Omega_e = 0.38$) predicted by the linear theory (Figures 8b and 8c). The upper-band waves, whose wave number is almost twice that of lower-band waves, are then generated by the wave-wave coupling. This mechanism, named as lower band cascade, has already been analyzed in previous work (Chen et al., 2017; Gao et al., 2016, 2017), and we will not describe its details.

In Table 2, we have listed the cases with the different plasma betas and temperature anisotropies of warm electrons, in which the whistler-mode spectrum with a power gap at about $0.5\Omega_e$ can be generated. The blue or red color indicates the most unstable whistler-mode belongs to the lower band or upper band. The results reveal that, when the frequency of the dominant wave mode ranges from ~ 0.5 to $\sim 0.6\Omega_e$, the spectrum will drift to the lower band. Then, a gap around $0.5\Omega_e$ will be formed due to the damping process caused by the beam-like/plateau electron population. When the frequency of the dominant mode is in the range of ~ 0.3 to $\sim 0.4\Omega_e$, the upper band can be driven by lower-band waves due to the lower band cascade, and a power gap is naturally formed between two bands. While, when the frequency ranges from $\sim 0.4\Omega_e$ to $\sim 0.5\Omega_e$, the process is complicated since both mechanisms can take effects, and a three-band wave may be generated consequently (not shown here).

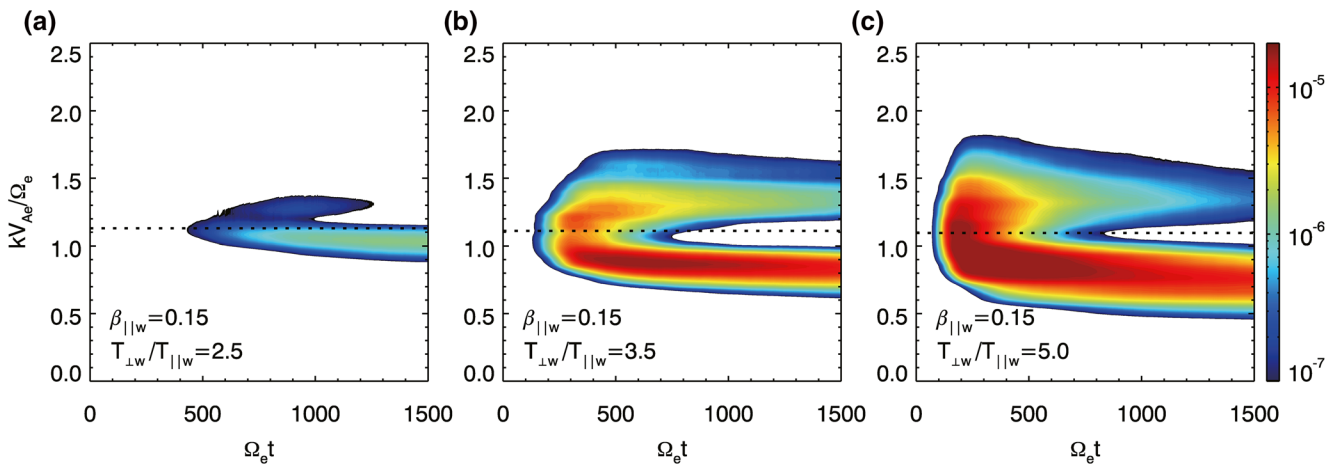


Figure 7. The k - t spectrogram of $\delta B_t^2 / B_0^2$ for the cases with (a) $T_{\perp w} / T_{||w} = 2.5$, (b) $T_{\perp w} / T_{||w} = 3.5$, and (c) $T_{\perp w} / T_{||w} = 5.0$, where the plasma beta is fixed at $\beta_{||w} = 0.15$. The dotted lines in three panels denote the wave numbers ($kV_{Ae} / \Omega_e = 1.130, 1.109$, and 1.095) corresponding to $0.5\Omega_e$ in each case.

Table 2

The Frequency ω / Ω_e of the Most Unstable Mode in Each Case, Under Different Temperature Anisotropy and Plasma Beta of the Warm Electrons

	$\beta_{\parallel w} = 0.09$	$\beta_{\parallel w} = 0.12$	$\beta_{\parallel w} = 0.15$	$\beta_{\parallel w} = 0.50$	$\beta_{\parallel w} = 0.55$	$\beta_{\parallel w} = 0.60$
$T_{\perp w} / T_{\parallel w} = 3.0$	0.547 ^a	0.527	0.507	0.394	0.381	0.370
$T_{\perp w} / T_{\parallel w} = 3.5$	0.566	0.540	0.521	0.401	0.389	0.377
$T_{\perp w} / T_{\parallel w} = 4.0$	0.575	0.553	0.530	0.403	0.391	0.379
$T_{\perp w} / T_{\parallel w} = 5.0$	0.590	0.561	0.537	0.409	0.396	0.374

^aThe generation mechanisms of two-band spectrum in each case are distinguished by different colors. The red color means the power gap is caused by the severe damping around $0.5\Omega_e$. While the blue color represents the banded structure is associated with the lower band cascade.

4. Summary and Discussion

With a 1-D PIC simulation model, we have investigated the generation mechanism of whistler-modes with a clear power gap around $0.5\Omega_e$, which have been ubiquitously observed in the inner magnetosphere. When the frequencies of excited waves in the linear stage cross $0.5\Omega_e$, or when they are slightly larger than but then drift to smaller than $0.5\Omega_e$, a pronounced beam-like/plateau component at about $\pm 0.5V_{Ae}$ is formed due to the Landau resonance. Such a component causes the severe damping around $0.5\Omega_e$ via cyclotron resonance and the power gap forms eventually. The parameter survey shows that the power gap can be generated by such a process related to the Landau resonance as the dominant frequency is in the range of ~ 0.4 to $\sim 0.6\Omega_e$. Moreover, a power gap can also be formed due to the lower band cascade when the dominant frequency ranges from ~ 0.3 to $\sim 0.4\Omega_e$.

In our simulations, the excited whistler waves can exhibit different types of spectra by changing initial plasma condition, which is similar to those detected by Van Allen Probes (VAP) in the Earth's magnetosphere. Figure 9 illustrates four whistler-mode wave events captured by VAP. If the linear growth rate peaks at a frequency much higher than $0.5\Omega_e$, then the excited whistler waves may only exist in a single band with frequency higher than $0.5\Omega_e$ (Figure 6a), just like the whistler wave in Figure 9a. If the initial plasma parameters fall in Table 2, then the banded whistler spectrum will be formed by either the beam-like/plateau electrons (Figure 1a) or lower band cascade (Figure 8a), which resembles the whistler event in

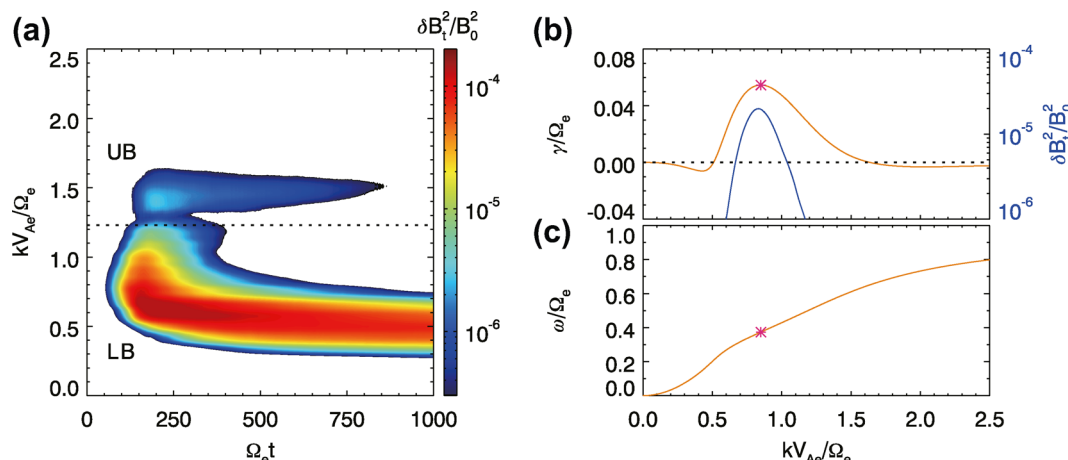


Figure 8. (a) The k - t spectrogram of $\delta B_t^2 / B_0^2$, the (b) growth rate and (c) dispersion relation of whistler-mode waves calculated by the linear theory, presented in the same format as that in Figure 1. The black dotted line in Figure 8a marks the wave number $kV_{Ae} / \Omega_e = 1.22$ corresponding to $0.5\Omega_e$, and the blue line in Figure 8c represents $\delta B_t^2 / B_0^2$ as a function of kV_{Ae} / Ω_e at $\Omega_e t = 120$.

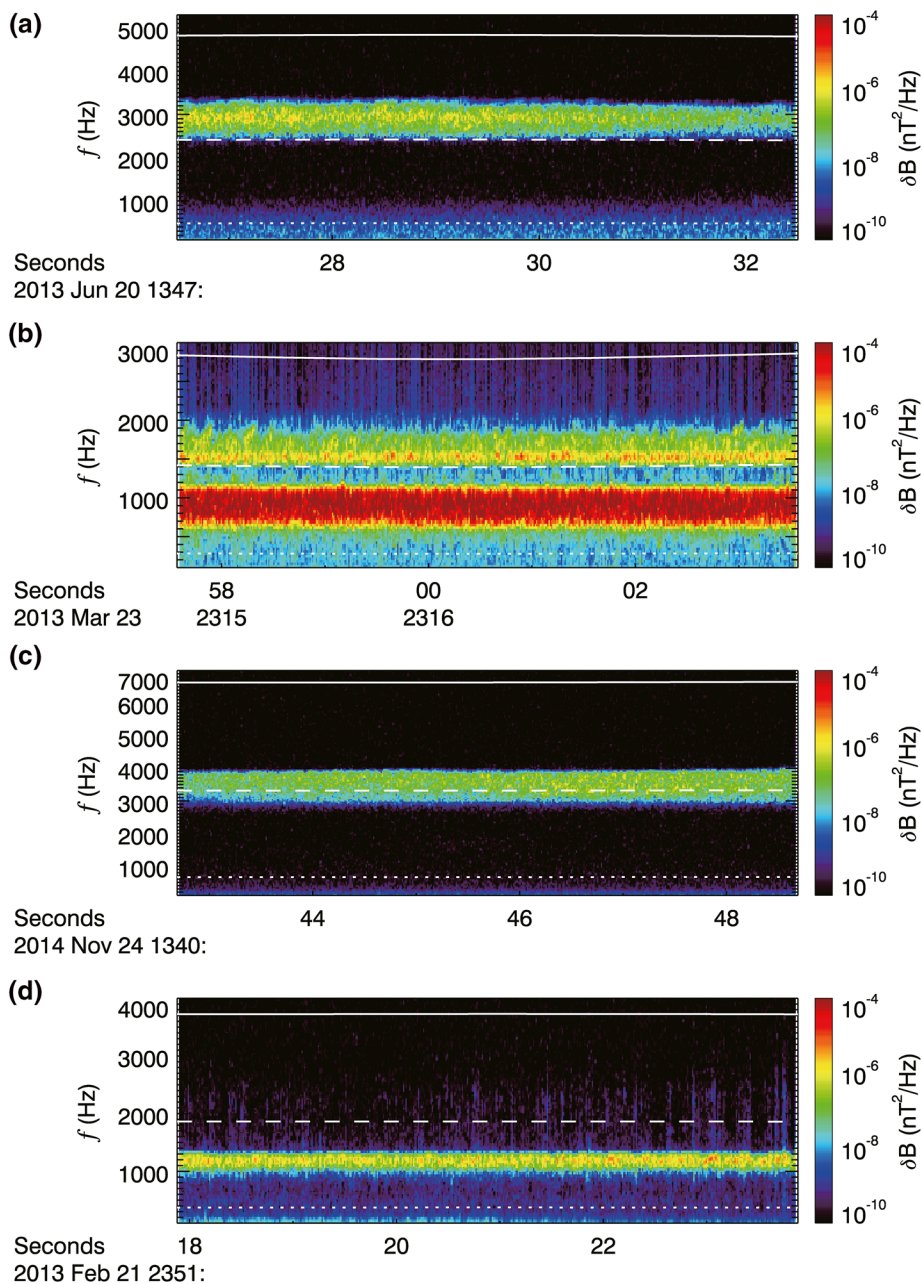


Figure 9. Four whistler-mode wave events showing the wave spectra: (a) only in the frequency band higher than $0.5\Omega_e$, (b) both in the upper band and in the lower band, (c) in one continuous band, and (d) only in the frequency band lower than $0.5\Omega_e$, which are all captured by Van Allen Probes. The full, dashed, and dotted lines in the four panels represent the frequencies $\omega = 0.8\Omega_e$, $0.5\Omega_e$, and $0.1\Omega_e$, respectively.

Figure 9b. However, in such cases, the continuous whistler spectrum can also be found in the early stage, such as $\Omega_e t = 150 - 400$ in Figure 7c, which is also observed in the magnetosphere (Figure 9c). Finally, if the upper-band waves are excited with small amplitudes, then they will be damped rapidly, and only a single frequency band lower than $0.5\Omega_e$ appears, like the wave spectrum in Figure 7a (Figure 9d).

With EPOCH 2-D simulations, Ratcliffe and Watt (2017) have also studied the generation of two-band whistler waves. They proposed that the modulation of velocity distribution is generated by the Landau resonance between electrons and strong wave mode around $0.5\Omega_e$, which can lead to the formation of a power gap. In

our study, we have shown that the beam-like/plateau electron distribution can play a key role in gap formation. Moreover, the beam-like/plateau shape can still be formed even though the wave at $0.5\Omega_e$ is not the most unstable mode. It should be caused by the Landau resonance between electrons and whistler modes within a large frequency range (not only the wave at $0.5\Omega_e$), since these waves have nearly the same phase velocity, i.e., $\sim 0.5V_{Ae}$.

Ratcliffe and Watt (2017) have initialized the simulation model by two anisotropic electron populations to excite both lower-band and upper-band waves. However, the constraint on the initial electron distribution can be further relaxed. In our simulations, there is one single anisotropic electron population. The pronounced beam-like/plateau shape is formed due to the Landau resonance, and can cause the severe damping around $0.5\Omega_e$. We have demonstrated that this mechanism will happen when the dominant frequency ranges from ~ 0.4 to $\sim 0.6 \Omega_e$. Moreover, the banded structure can also be generated by the lower band cascade, when the dominant frequency is in the range of ~ 0.3 to $\sim 0.4\Omega_e$.

Omura et al. (2009) and Hsieh and Omura (2018) suggested the whistler waves excited in the equator region will experience nonlinear damping via the Landau resonance around $0.5\Omega_e$ as they propagate to the higher latitudes, which implies the banded waves preferentially appear at larger magnetic latitudes. However, a recent statistical study (Gao et al., 2019) reveals that banded whistler events tend to be observed near the magnetic equator, i.e., within the source region. Besides, how the Landau resonance affects the evolution of whistler waves in a self-consistent system is still unclear. In our simulation, the power gap forms at about $450\Omega_e^{-1}$ (Figure 1a), corresponding to about 0.0273 s at L -shell = 7, which means the whistler waves only propagate $\sim 1.31^\circ$ away from the magnetic equator. Therefore, our study can well explain why the banded whistler waves preferentially appear near the magnetic equator. Besides, whistler-mode whistler waves are usually observed in association with the beam-like/plateau electron component in the magnetosphere (Chen et al., 2019; Li et al., 2019). In our study, the number density percentage of beam-like/plateau component is only $\sim 10^{-3}$, but this tenuous component can cause severe damping at $0.5\Omega_e$, leading to the formation of power gap. According to the study by Chen et al. (2019), the number density percentage of beam-like/plateau electrons along with whistler wave ranges from 10^{-4} to 10^{-2} in Earth's magnetosphere, which provides strong support to our mechanism.

In this study, for saving computation time and space, we have employed a 1-D PIC simulation model since we can set more particles in each cell to reduce the background noise. Besides, whistler-mode waves in the Earth's magnetosphere are typically observed to have finite wave normal angles (mainly smaller than 30° , Gao et al., 2018; Li et al., 2011). As a result, we artificially fix the wave normal by using the 1-D PIC simulation model. In fact, other wave normal angles have also been simulated and the results remain almost unchanged. However, the real space is an open system in the dipole magnetic field. Therefore, a 2-D PIC simulation model with the dipole field should be required and will be employed in the future.

Data Availability Statement

The simulation data are archived in <https://dx.doi.org/10.12176/01.99.00161>. The VAP data used here, obtained from <https://spdf.sci.gsfc.nasa.gov/pub/data/rbsp>.

References

- Birdsall, C. K., & Langdon, A. B. (1991). *Plasma physics via computer simulation*. Philadelphia, PA: IOP Publishing. <https://doi.org/10.1887/0750301171>
- Burtis, W. J., & Helliwell, R. A. (1969). Banded chorus a new type of VLF radiation observed in the magnetosphere by OGO 1 and OGO 3. *Journal of Geophysical Research*, 74(11), 3002–3010. <https://doi.org/10.1029/JA074i011p03002>
- Chen, H. Y., Gao, X. L., Lu, Q. M., Ke, Y. G., & Wang, S. (2017). Lower band cascade of whistler waves excited by anisotropic hot electrons: One dimensional PIC simulations. *Journal of Geophysical Research: Space Physics*, 122, 10448–10457. <https://doi.org/10.1002/2017JA024513>
- Chen, H., Gao, X., Lu, Q., Sun, J., & Wang, S. (2018). Nonlinear evolution of counter-propagating whistler mode waves excited by anisotropic electrons within the equatorial source region: 1-D PIC simulations. *Journal of Geophysical Research: Space Physics*, 123(2), 1200–1207. <https://doi.org/10.1002/2017JA024850>
- Chen, R., Gao, X., Lu, Q., & Wang, S. (2019). Unraveling the correlation between chorus wave and electron beam-like distribution in the Earth's magnetosphere. *Geophysical Research Letters*, 46(21), 11671–11678. <https://doi.org/10.1029/2019GL085108>

Acknowledgments

This work was supported by the NSFC grant 41774151, 41527804, 41631071, Young Elite Scientists Sponsorship Program by CAST (2018QNRC001), Key Research Program of Frontier Sciences, CAS(QYZDJ-SSW-DQC010), the Fundamental Research Funds for the Central Universities and B-type Strategic Priority Program of the Chinese Academy of Sciences, Grant No. XDB41000000. We acknowledge for the data resources from 'National Space Science Data Center, National Science & Technology Infrastructure of China (<http://www.nssdc.ac.cn>). The authors also acknowledge the entire VAP instrument team.

- Chen, L. J., Thorne, R. M., Li, W., & Bortnik, J. (2013). Modeling the wave normal distribution of chorus waves. *Journal of Geophysical Research*, 118, 1074–1088. <https://doi.org/10.1029/2012JA018343>
- Fu, X., Cowee, M. M., Friedel, R. H., Funsten, H. O., Gary, S. P., Hospodarsky, G. B., et al. (2014). Whistler anisotropy instabilities as the source of banded chorus: Van Allen Probes observations and particle-in-cell simulations. *Journal of Geophysical Research: Space Physics*, 119, 8288–8298. <https://doi.org/10.1002/2014JA020364>
- Gao, X., Chen, L., Li, W., Lu, Q., & Wang, S. (2019). Statistical results of the power gap between lower-band and upper-band chorus waves. *Geophysical Research Letters*, 46, 4098–4105. <https://doi.org/10.1029/2019GL082140>
- Gao, X., Ke, Y., Lu, Q., Chen, L., & Wang, S. (2017). Generation of multiband chorus in the Earth's magnetosphere: 1-D PIC simulation. *Geophysical Research Letters*, 44, 618–624. <https://doi.org/10.1002/2016GL072251>
- Gao, X., Li, W., Thorne, R. M., Bortnik, J., Angelopoulos, V., Lu, Q., et al. (2014). New evidence for generation mechanisms of discrete and hiss-like whistler mode waves. *Geophysical Research Letters*, 41, 4805–4811. <https://doi.org/10.1002/2014GL060707>
- Gao, X. L., Lu, Q. M., Bortnik, J., Li, W., Chen, L. J., & Wang, S. (2016). Generation of multiband chorus by lower band cascade in the Earth's magnetosphere. *Geophysical Research Letters*, 43, 2343–2350. <https://doi.org/10.1002/2016GL068313>
- Gao, X., Lu, Q., & Wang, S. (2018). Statistical results of multiband chorus by using THEMIS waveform data. *Journal of Geophysical Research: Space Physics*, 123, 5506–5515. <https://doi.org/10.1029/2018JA025393>
- Hsieh, Y.-K., & Omura, Y. (2018). Nonlinear damping of oblique whistler mode waves via Landau resonance. *Journal of Geophysical Research: Space Physics*, 123(9), 7462–7472. <https://doi.org/10.1029/2018JA025848>
- Li, J., Bortnik, J., An, X., Li, W., Angelopoulos, V., Thorne, R. M., et al. (2019). Origin of two-band chorus in the radiation belt of Earth. *Nature Communications*, 10(1), 4672. <https://doi.org/10.1038/s41467-019-12561-3>
- Li, W., Bortnik, J., Thorne, R. M., & Angelopoulos, V. (2011). Global distribution of wave amplitudes and wave normal angles of chorus waves using THEMIS wave observations. *Journal of Geophysical Research*, 116, A12205. <https://doi.org/10.1029/2011JA017035>
- Liu, K., Gary, S. P., & Winske, D. (2011). Excitation of banded whistler waves in the magnetosphere. *Geophysical Research Letters*, 38, L14108. <https://doi.org/10.1029/2011GL048375>
- Lu, Q., Ke, Y., Wang, X., Liu, K., Gao, X., Chen, L., & Wang, S. (2019). Two-dimensional general curvilinear particle-in-cell (gcPIC) simulation of rising-tone chorus waves in a dipole magnetic field. *Journal of Geophysical Research: Space Physics*, 124, 4157–4167. <https://doi.org/10.1029/2019JA026586>
- Lu, Q., Wang, L., Zhou, Y., & Wang, S. (2004). Electromagnetic instabilities excited by electron temperature anisotropy. *Chinese Physics Letters*, 21(1), 129. <https://doi.org/10.1088/0256-307X/21/1/039>
- Ni, B., Thorne, R. M., Shprits, Y. Y., & Bortnik, J. (2008). Resonant scattering of plasma sheet electrons by whistler-mode chorus: Contribution to diffuse auroral precipitation. *Geophysical Research Letters*, 35, L11106. <https://doi.org/10.1029/2008GL034032>
- Omura, Y., Hikishima, M., Katoh, Y., Summers, D., & Yagitani, S. (2009). Nonlinear mechanisms of lower-band and upper-band VLF chorus emissions in the magnetosphere. *Journal of Geophysical Research*, 114, A07217. <https://doi.org/10.1029/2009JA014206>
- Ratcliffe, H., & Watt, C. E. J. (2017). Self-consistent formation of a 0.5 cyclotron frequency gap in magnetospheric whistler mode waves. *Journal of Geophysical Research: Space Physics*, 122, 8166–8180. <https://doi.org/10.1002/2017JA024399>
- Santolik, O., Gurnett, D. A., Pickett, J. S., Parrot, M., & Cornilleau-Wehrlin, N. (2005). Central position of the source region of storm-time chorus. *Planetary and Space Science*, 53(1–3), 299–305. <https://doi.org/10.1016/j.pss.2004.09.056>
- Santolik, O., Gurnett, D. A., Pickett, J. S., Parrot, M., & Cornilleau-Wehrlin, N. (2003). Spatio-temporal structure of storm-time chorus. *Journal of Geophysical Research*, 108(A7), 1278. <https://doi.org/10.1029/2002JA009791>
- Sauer, K., Baumgärtel, K., & Sydora, R. (2020). Gap formation around $\Omega_e/2$ and generation of low-band whistler waves by Landau-resonant electrons in the magnetosphere: Predictions from dispersion theory. *Earth and Planetary Physics*, 4(2), 1–13. <http://doi.org/10.26464/epp20200020>
- Sydora, R. D., Sauer, K., & Silin, I. (2007). Coherent whistler waves and oscilliton formation: Kinetic simulations. *Geophysical Research Letters*, 34, L22105. <https://doi.org/10.1029/2007GL031839>
- Terasawa, T., Hoshino, M., Sakai, J. I., & Hada, T. (1986). *Journal of Geophysical Research*, 91(A4), 4171–4187. <https://doi.org/10.1029/JA09liA04p04171>
- Thorne, R. M., Li, W., Ni, B., Ma, Q., Bortnik, J., Chen, L., et al. (2013). Rapid local acceleration of relativistic radiation-belt electrons by magnetospheric chorus. *Nature*, 504(7480), 411–414. <https://doi.org/10.1038/nature12889>
- Thorne, R. M., Ni, B., Tao, X., Horne, R. B., & Meredith, N. P. (2010). Scattering by chorus waves as the dominant cause of diffuse auroral precipitation. *Nature*, 467(7318), 943–946. <https://doi.org/10.1038/nature09467>
- Tsurutani, B. T., & Smith, E. J. (1974). Postmidnight chorus: A substorm phenomenon. *Journal of Geophysical Research*, 79(1), 118–127. <https://doi.org/10.1029/JA079i001p00118>
- Xiao, F., Yang, C., He, Z., Su, Z., Zhou, Q., He, Y., et al. (2014). Chorus acceleration of radiation belt relativistic electrons during March 2013 geomagnetic storm. *Journal of Geophysical Research: Space Physics*, 119, 3325–3332. <https://doi.org/10.1002/2014JA019822>
- Xie, H., & Yong, X. (2016). PDRK: A general kinetic dispersion relation solver for magnetized plasma. *Plasma Science and Technology*, 18(2), 97–107. <https://doi.org/10.1088/1009-0630/18/2/01>